1-1-2007

Simulation of dynamic recrystallization using irregular cellular automata

N Yazdipour
University of Wollongong, nimayaz@uow.edu.au

A Dehghan-Manshadi
Deakin University, alidm@uow.edu.au

C H. J Davies
Monash University

P D. Hodgson
Deakin University

MATERIALS FORUM VOLUME 31 - 2007
Edited by J.M. Cairney and S.P. Ringer

SIMULATION OF DYNAMIC RECRYSTALLIZATION USING IRREGULAR CELLULAR AUTOMATA

N. Yazdipour[1], A. Dehghan-Manshadi[1], C. H. J. Davies[2], P.D. Hodgson[1]

[1]Centre of Material and Fibre Innovation (CMFI), Deakin University, Geelong, Victoria 3217, Australia
[2]School of Physics and Materials Engineering, Monash University, Victoria 3800, Australia

ABSTRACT

Computer simulation is a powerful tool to predict microstructure and its evolution during dynamic recrystallization. Cellular Automata (CA), as one of the most efficient methods proposed to simulate recrystallization and grain growth. In this work, recrystallization and grain growth phenomena were modelled by using a two dimensional irregular CA method. Initial grain size, nuclei density and orientation of each grain were variables which have been used as entering data to the CA model. Final grain size, orientation of each grain, dislocation density and stress-strain curve were the results which have been resulted to validate the current model. Considering the model assumptions, it is shown that the CA can successfully simulate dynamic recrystallization.

Key Words: Dynamic recrystallization, dislocation density, irregular cellular automata

1. INTRODUCTION

Hot deformation and its dependent phenomena, such as dynamic recrystallization (DRX) and dynamic recovery (DRV) have been the subject of many studies [1]. In addition to experimental methods, simulation has always been used as a quick and accurate approach to these studies. However, the simulation of DRX has been attracted the most attention during the last decade [2, 3]. The ideal homogeneous recrystallization has been modelled using the JMAK theory [4] but, in real materials, the ideal JMAK behaviour is rarely observed because of the heterogeneous nature of recrystallization. So, a method was required to model recrystallization properly. Cellular automata (CA) method gives a time and space dependent description of recrystallization. As a numerical approach, CA provides a virtual visible evolution of the microstructure during recrystallization [3].

In this study, dynamic recovery was modelled by the Estrin-Mecking method to predict the three main stresses (critical, peak and steady state stresses) on the flow curve. Then an approach utilized to relate the three stresses to Zener-Hollomon parameter (Z) and the results of this approach were compared to the Poliak's approach [5]. In the CA approach, the volume fraction of recrystallized material was derived by using a new neighbouring method called random CA. Finally, the CA results have been compared to the experiments and the flow curve, final microstructure, final grain size and DRX volume fraction were obtained from the CA model.

2. ESTRIN-MECKING METHOD

Dislocation density during hot deformation depends on two competing processes: work hardening and softening (including dynamic recovery and recrystallization). Two approaches have been suggested to analyse work hardening: the "Kocks-Mecking" (KM) [6] and the "Estrin-Mecking" (EM) [7] methods. Both are based on the assumption that the plastic flow kinetics are determined by a single parameter [7] of the dislocation density (ρ). In the former method, it was assumed that after moving a distance proportional to $\rho^{1/2}$, dislocations stopped moving. But, the assumption that the mean free path of dislocations is proportional to $\rho^{-1/2}$ was rejected by the Estrin-Mecking method [8] when the spacing between obstacles determine the mean free path. Estrin and Mecking assumed that the distance is a geometrically determined quantity which depended on the particle spacing or grain size (*d*). As the material used in this study (304 SS) previously followed the EM method[8, 9], this method is used to predict DRV.

In the EM approach, the first term of dislocation evolution (Equation.1) [10] which expressing the athermal storage rate is constant and the change of $\rho^{1/2}$ with time is zero and the mean free path is assumed constant. Therefore, the EM equation follows as:

$$\frac{d\rho}{d\varepsilon} = K_1 - K_2\rho \qquad \textbf{(1)}$$

where K_1 is determined by the constant mean free path:

$$K_1 = \frac{1}{bl} \qquad \textbf{(2)}$$

and K_2 is a function for temperature and strain rate, $K_2 = f(T, \dot{\varepsilon})$ [8]. The following approach shows the relation between the constants and thermomechanical parameters. Dislocation density was related to stress through $\sigma = \sigma_0 + \alpha G b\sqrt{\rho}$ in which α is a dislocation

interaction term and is constant for most metals, G is the shear modulus and b is the Burgers vector [11]. It was assumed that at the beginning of deformation, when strain is zero, the stress is equal to the initial one. While, after passing steady state stress the strain will not change any more. Therefore, the boundary conditions were defined as:

$$\begin{cases} \sigma = \sigma_0 \Leftrightarrow \varepsilon = 0 \\ \sigma = \sigma_{ss} \Leftrightarrow \varepsilon = \infty \end{cases} \quad \textbf{(3)}$$

Therefore, the stress can be expressed with the following equation:

$$\sigma = \sigma_0 + \sqrt{\frac{A}{B}\left[1 - \exp\left(-2B\varepsilon\right)\right]} \quad \textbf{(4)}$$

where $A = \frac{K_1}{2}\left(\alpha G b\right)^2$, $B = \frac{K_2}{2}$.

So, by identifying the temperature and strain rate, the stress-strain curve which shows dynamic recovery can be plotted through Equation 4.

3. EXPERIMENTAL PROCEDURES

The material used in this study was AISI 304 austenitic stainless steel. Its chemical composition is given in the Table 1. To achieve recrystallization, various thermomechanical schedules were utilized by hot torsion test. The torsion rig and its specifications were explained before [12].

Table 1 Chemical composition of the 304 SS used in the current study (wt%)

Alloy	**C**	**Mn**	**Si**	**P**	**S**
	0.02	1.6	0.7	0.03	0.01
304 SS	**Ni**	**Cr**	**Mo**	**Cu**	
	8.2	18.5	0.1	0.8	

The torsion program is illustrated in Figure 1. Since, the model was verified by using two different initial grain sizes, the second program was considered to achieve another fully recrystallized microstructure with different initial grain size (20 μm) by applying an extra deformation at 900 ^{o}C before the final hot deformation test. Also, different strain rates applied on the material to consider the effect of strain rate (Figure 2). To study the microstructure, common metallographic preparation was carried out on the samples and their microstructure were analysed by EBSD.

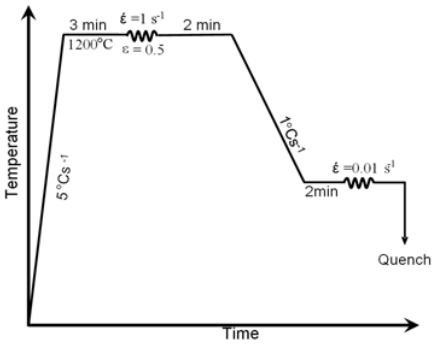

Figure 1. Schematic diagram of hot torsion schedule used in this work.

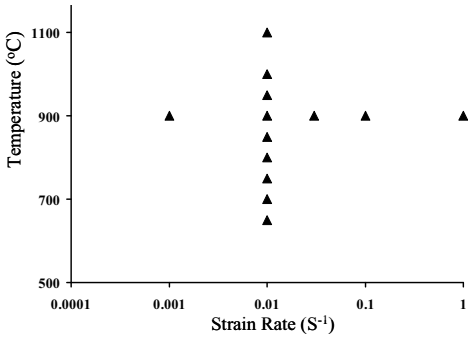

Figure 2. Matrix of strain rates used in this work

4. EEPERIMENTAL RESULTS

4.1 Flow Curve

As explained, hot torsion test was performed on 304 austenite stainless steel samples for different temperatures and strain rates (Figures 3.a,b).

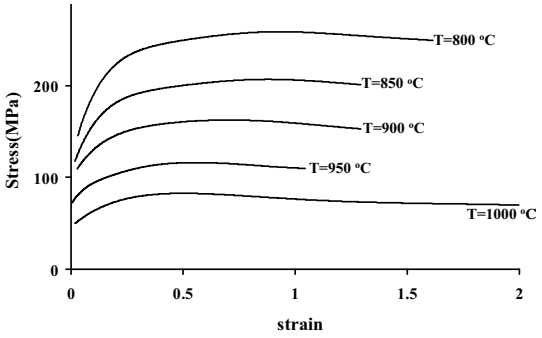

(a)

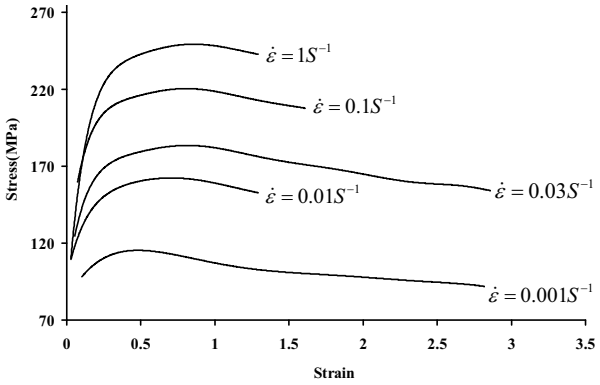

(b)

Figure 3. Stress-strain curves from torsion test at (a) constant strain rate ($0.01S^{-1}$) and (b) at constant temperature (900 ^{o}C).

At low temperatures (e.g. lower than 800°C), the peak stress was eliminated and the flow stress was gradually increased. For temperatures close to 700 ^{o}C, the peak stress was equal to the steady state stress and the latter stress could not be distinguished from the former one. Therefore, 700 ^{o}C was assumed the dynamic recovery temperature of this material (Figure 4).

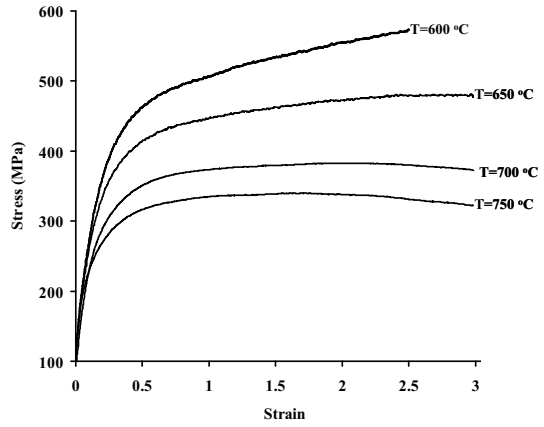

Figure 4. Flow curves of 304 stainless steel at constant strain rate (0.01 S^{-1}) at different temperatures.

4.2 Work Hardening Curve

It is assumed that DRX initiates after passing a critical stress in the flow stress curve. Therefore, knowing this stress is important. There are two methods to measure critical stress or the initiation point of recrystallization, through either flow curve or microstructure analysis. Since, there are many difficulties to use the latter method such as obtaining high quality images and large quantity of samples, the flow stress analysis is preferable. When recrystallization occurs, the flow curve and consequently the work hardening curve ($\theta(=d\sigma/d\varepsilon)-\sigma$) change (Figure 5). This approach was first used by Estrin [13] and then continued by McQueen and Ryan [14, 15]. In this approach, the onset of DRX was defined by the deviation in the work hardening curves. It was assumed that the critical stress is the position on the flow curve that at least % 2 of microstructure was recrystallized and makes a visible change in the flow curve [16].

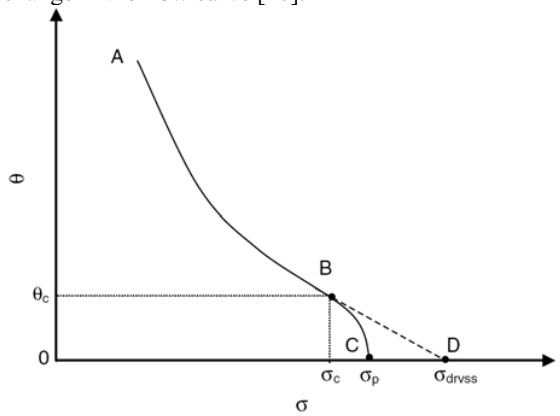

Figure 5. Schematic representation of the work hardening versus stress graph for dynamically recovered (ABD) and dynamically recrystallized (ABC) material [13].

As shown in Figure 5, the work hardening curve is composed of two stages. In the first stage, with increasing stress the work hardening rate decreased rapidly due to the dynamic recovery. Then, the second part initiated where there is an obvious change in the slope of the curve. It was assumed that DRX initiated at this point. By progressing deformation, the work hardening curve crosses the horizontal axis (θ =0). The point that the curve met the horizontal axis is the condition in which the work hardening rate became zero, that is, the hardening and softening rate are equal. This point (point C in Figure 5) is the peak stress, σ_p, where softening by DRV and DRX is equal to the hardening due to the deformation. By following the first section of the curve as a straight line (the dashed line in Figure 5), the crossing point is the saturation stress equal to the steady state or dynamic recovery stress (point D in Figure 5).

By following the Poliak approach, the work hardening curves have been plotted from the flow curves for different temperature and strain rates (Figures 6). The critical stresses in different deformation conditions which were obtained from the work hardening curves by using the Estrin-Mecking approach is located on a straight line (Figure 6.a) [5].

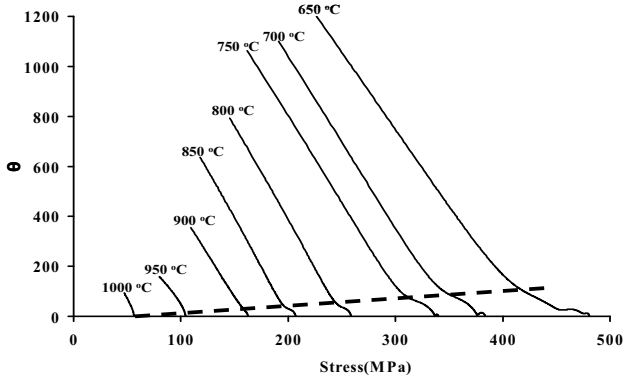

(a)

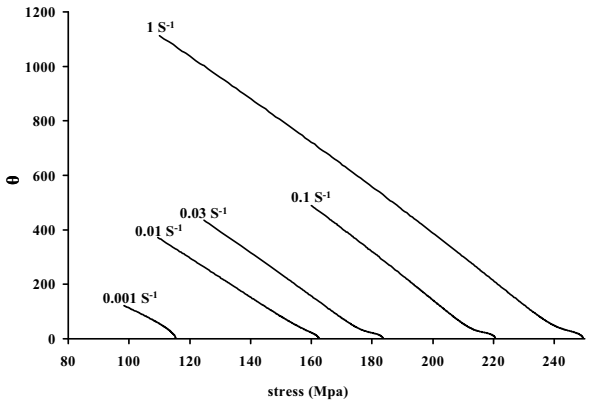

(b)

Figure 6. θ-σ curve in different thermomechanical conditions. (a) at constant strain rates (0.01 S^{-1}) and (b) at constant temperature (900 ^{o}C).

By following the Poliak approach, critical (σ_c), peak (σ_p) and steady state (σ_{drvss}) stresses were calculated for different temperatures and strain rates and are summarized in table 2.

Table 2 Critical, peak and steady state stresses in different thermomechanical conditions

$\dot{\varepsilon}$ (s^{-1})	T(^{o}C)	σ_c	σ_p	σ_{drvss}
0.001	900	108	115.34	120
0.01	900	161	162.45	164.4
0.03	900	181.4	183.5	188.4
0.1	900	218.1	220.5	227
1	900	246.6	249.5	255.1
0.01	750	327	336.5	351.5
0.01	775	276.8	284	300
0.01	800	252.4	258	271
0.01	850	203.7	206.5	215.2
0.01	950	108.3	116	127
0.01	1000	75.2	82.6	87.2
0.01	1100	54.6	56.2	57.6

4.3 Critical, Peak and Steady State Stresses

The critical stress, σ_{cr}, is the point after which the DRX initiated when dislocation density exceeded the critical one and misorientation between neighbouring grains exceeded 15^{o}. Also, this is the point that DRV and DRX curves started deviating from each other. It is shown that critical stress in various thermomechanical conditions can be expressed through Zener-Hollomon parameter (Equation 5) (Figure 7).

$$\sigma_c = 0.52(Z)^{0.1206} \quad \textbf{(5)}$$

Peak stress is the position on the flow curve in which dislocation generation (due to deformation) is equal to the dislocation annihilation (due to recovery and recrystallization). Therefore, the flow curve will follow a flat route (in DRV) and will drop (in DRX). When DRX is the dominant mechanism during deformation, peak stress can be identified clearly while hardening is the main mechanism, the volume fraction of recrystallized microstructure will become lower and the consequent softening will not be so strong to equalize hardening. Therefore, the peak stress would not be distinguished easily. Regardless of Z value, it is shown that the experimental results have a good agreement with the numerical approach (Figure 7) and peak stress has been expressed by Zener-Hollomon parameter as well.

$$\sigma_p = 1.31(Z)^{0.13} \quad \textbf{(6)}$$

As shown in Figure 3.a (i.e. in the case of 1000 ^{o}C) and after passing a special strain, there is no change in the stress. This means there is equilibrium between dislocation generation and annihilation. The point after which the stress will not change any longer while strain is increasing is defined as steady state stress, σ_{ss}, [17]. When recrystallization happened, the stress dropped evidently and flattened up to the end of the deformation and the Z value affected the shape of the flow curve and the position of the peak stress. The same event occurred for the steady state stress but in this case, a fully recrystallized microstructure was obtained while in the two previous cases it was impossible to achieve a fully recrystallized microstructure. Roucoules demonstrated that steady state stress depended only on the Z value [18].

$$\sigma_{ss} = 7.2Z^{0.09} \quad \textbf{(7)}$$

The numerical approach also showed that steady state stress is dependent upon Zener-Hollomon (Equation 8).

$$\sigma_{ss} = 0.5361(Z)^{0.1122} \quad \textbf{(8)}$$

As Roucoules showed, the first constant depended on the material properties. Thus, there would be reasonable to be different from the constant derived form numerical approach but the second constants in Equations 7, 8 (the exponents) are fairy close to each other.

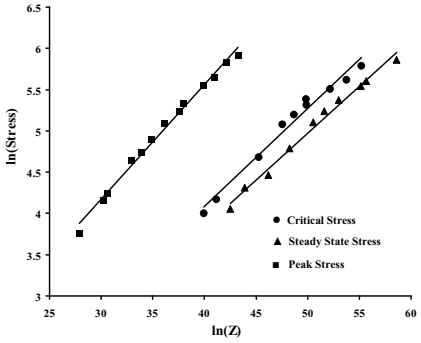

Figure 7. Dependence of critical, peak and steady state stresses to the Zener-Hollomon parameter ($Q_{def.}$=400 kJ/mol K)

5. "THREE-STRESS" APPROACH

By applying equations 5, 6 and 8, it would be possible to predict three stresses (critical, peak and steady state) under various thermomechanical conditions (including temperature and strain rate). So, by having three important points of the flow curve, it would be possible to plot the DRV curve (Figure 8.a). When the CA model ran, recrystallization initiated and continued up to the point where the whole microstructure would be fully recrystallized. At this point the stress was equal to the steady state value. So, during recrystallization, the volume fraction of recrystallized microstructure could be calculated in each time increment and the final outline have had a "S" shape curve (Figure 8.b) [19]. By considering Figures 8.a and b together, the dynamic recrystallization curve can be derived (Figure 8.c).

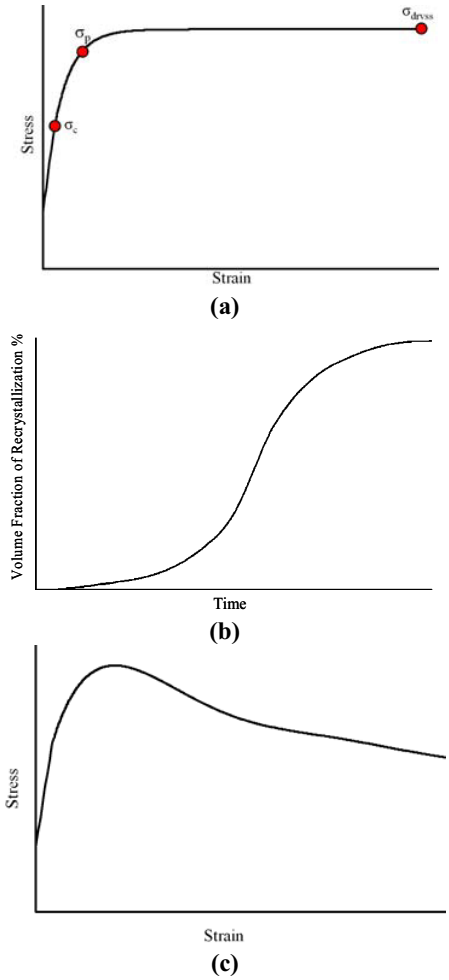

Figure 8. Schematic dynamic recovery curve (a), typical "S" shape of volume fraction percentage of recrystallized microstructure (b), Schematic dynamic recrystallization curve (c).

Then, the EM approach has been used to compare the dynamic recovery results obtained from numerical approach with the EM method. The Figure 9 illustrates the results for different deformation conditions. It is obvious that EM approach predicted the DRV curve in various thermomechanical conditions properly. By comparing the results in different thermomechanical conditions, it was shown that in high strain rates the numerical approach did not give the accurate results as it gave in the lower strain rates (Figure 9.a,b). However, the approach gave precise results in different temperatures (Figure 9.c,d). This means that the approach is much more sensitive to the strain rate than to the temperature because of activating different deformation mechanisms.

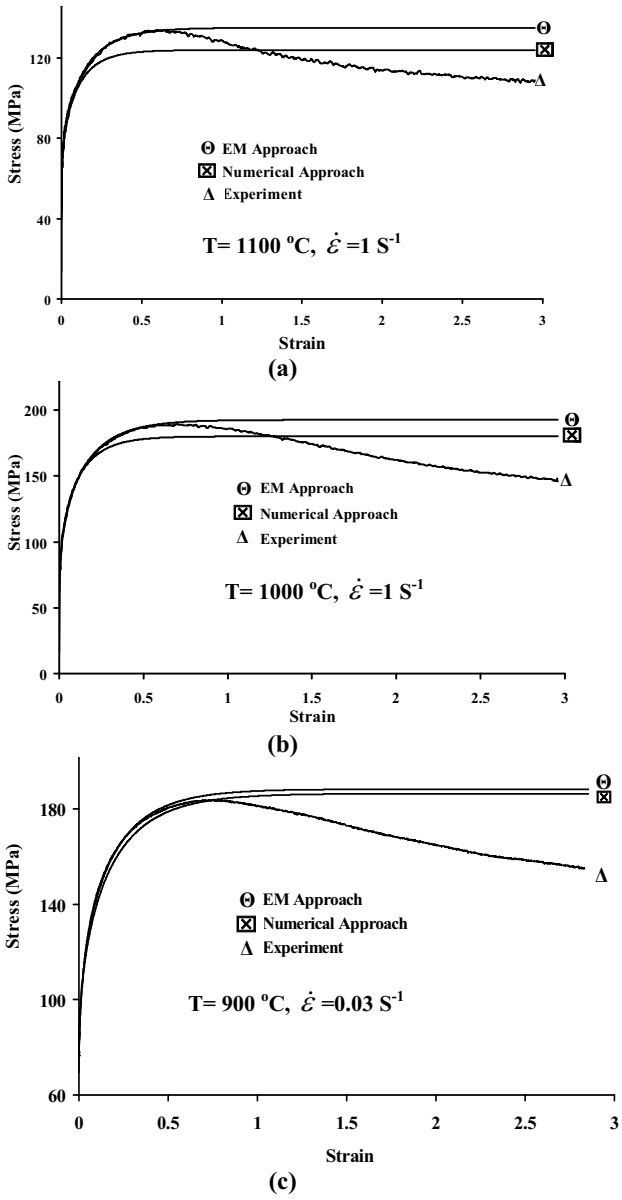

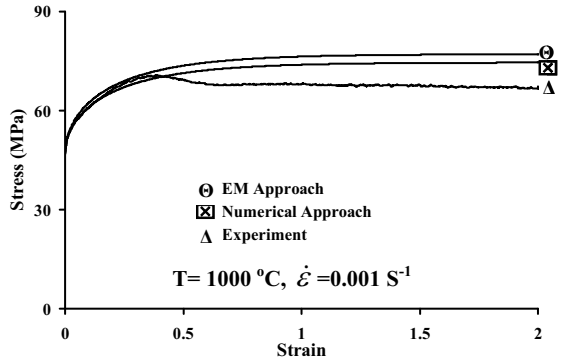

(d)

Figure 9. stress-strain curves in different thermomechanical conditions to show comparisons between EM and numerical approach with DRV curves.

6. CELLULAR AUTOMATA METHOD

In the CA approach, each domain is divided into cells; each of them has a defined state. This state refers to the grain to which the cell belongs [19]. CA computes the evolving microstructure by updating the state of all cells; the new state depends on the state of cells in a defined neighbourhood. In conventional CA, an equi-distant grid is used [3]. While early work used a regular cell arrangement, recent developments have allowed the use of a random grid cellular automata [20]. CA approach gives a time and space dependent description of the recrystallization process. As a numerical approach, CA provides a virtual visible evolution of the microstructure during recrystallization. In many cases, local variations have a substantial influence on recrystallization and grain growth, and at the same time the heterogeneity of these local variations in the microstructure makes it difficult to include them in a statistical model. Techniques such as CA solve this problem simply by spatially resolving the microstructure[3].

Conventional CA as depicted (Figure 10.a,b), is equidistantly distributed over the microstructure volume [2]. This equidistant aspect of the cell distribution is the main reason why the link to time and space can not be made, obviously because the distances between the cells are not equal in all spatial directions due to their shape. Consequently, given the same conditions for driving force and mobility, the velocity of a grain boundary is directionally dependent on its relative orientation to the CA grid. A solution to this problem is the use of a randomly distributed grid Figure 10.c). On average, the distance between neighbouring cells in a random grid is independent of the spatial direction. Given the statistical isotropy of the neighbourhood of a cell, the problem is reduced to find a cell updating rule that couples CA algorithm to space and time dimensions. An additional advantage of a random grid is that, when the material is homogeneously deformed, it is still a random grid.

The notion of the spatial resolution of CA can be defined as the number of cells per unit area or unit volume. Fixed grid cellular automata have a constant resolution, which means there are no local changes in the cell density. The case for random grid automata is completely different, in which the number of cells per unit area varies according to the positions in the. The local variation of the cells density can affect the simulation in two ways. The first problem is that computational accuracy changes locally, it means that local density of the random grid have to consider accuracy. Neighbourhood definition of cells is the most important feature of computations. The status of a cell is updated and the new cell status depends on the status of the neighbouring cells [20]. In an equidistant square grid CA, the neighbourhood is typically defined to be the four (Von Neumann) or eight (Moore) adjacent neighbouring cells while it is completely dependent on the neighbourhood radius in random CA (Figure 10.c).

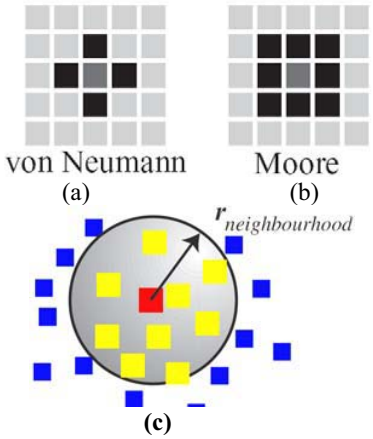

Figure 10. Neighbourhood definitions in conventional CA (a,b) and in random grid cellular automata (c)

In conventional CA all of the cells are updated in each time increment. The new status of each cell is calculated according to the present status of all cells located in its neighbourhood and then all cells receive their new status. In the random CA, the status of all cells in each time increment should be calculated but since during recrystallization, grain boundaries move in a fixed direction towards the deformed regions, it is not essential to update the status of all cells in each time step. The best modification is that cells whose status is recrystallized will be removed from the updating system. This approach eliminates the cells which have "recrystallized" status in previous steps from being updated.

6.1 Boundary Conditions

There are two approaches to define neighbourhood and transition rule for boundary points. One possibility is to have different transition rule for these locations, and another one is to expand the neighbourhood condition for these places. One of the most common solutions has been proposed as the periodic boundary condition in which one supposes that the lattice is embedded in a torus-like shape. In the case of the 2D lattice, this means that the right side of the domain is the rest of the

left side, and lower side is the rest of the upper side (Figure 11).

n,m	$n,0$	$\cdots$	n,j	$\cdots$	n,m	$n,0$
$0,m$	$0,0$	$\cdots$	$0,j$	$\cdots$	$0,m$	$0,0$
$\vdots$	$\vdots$	$\vdots$	$\vdots$	$\vdots$	$\vdots$	$\vdots$
i,m	$i,0$	$\cdots$	i,j	$\cdots$	i,m	$i,0$
$\vdots$	$\vdots$	$\vdots$	$\vdots$	$\vdots$	$\vdots$	$\vdots$
n,m	$n,0$	$\cdots$	n,j	$\cdots$	n,m	$n,0$
$0,m$	$0,0$	$\cdots$	$0,j$	$\cdots$	$0,m$	$0,0$

(a)

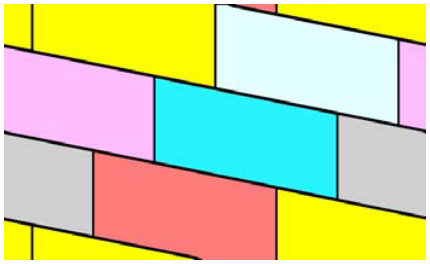

(b)

Figure 11. Periodic boundary condition, mathematically (a), imaginary (b).

In the current model, an initial microstructure which was composed of 100 × 100 cells was used to reduce the running time and memory usage. The first neighbourhood radius was defined by 3, but it could be changed as one of the initial entering variables in the model. In this model, it was assumed that all of the cells were identical; therefore, the critical dislocation density was equal to the critical dislocation density of each cell. The initial microstructure was generated by dispersing some nuclei randomly and letting them to grow to obtaining a fully impinged microstructure. In the initial microstructure, each grain was distinguished by two parameters; firstly, its own digit which was given to each cell and represents its orientation. The orientation value of each cell came from the average number of three digits which represented the colour of the cell (Figure 12.a) which was an integer in the range 1 to 180 degrees and secondly a grain boundary which was distinguished as a line between two different coloured-cells.

(a)

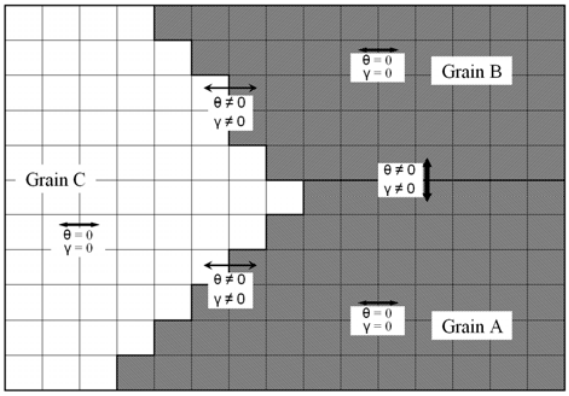

(b)

Figure 12. A typical initial microstructure in which each grain has its own colour (orientation) (a), different grains has different colours and different orientations.

It could be possible to consider grain boundaries as one or even two layers of cells but the problem emerged when one cell changed its state from an unrecrystallized cell to the recrystallized one. When a new nucleus nucleated, it should be distinguished from its surroundings by one (Figure 13.a) or two layers of cells (Figure 13.b) which was not reasonable and did not have any physical concept. Therefore, grain boundaries were distinguished as the interface between two different coloured-cells.

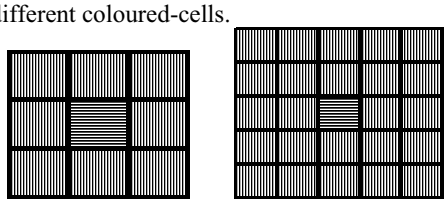

(a) (b)

Figure 13. Layers of grain boundary around one recrystallized cell. One layer (a) and two layers (b).

By assuming that "R","G" and "B" are representatives of red, green and blue, each cell has a specific colour and therefore has a specific orientation through the following equation:

$$\varphi = \left[\left(R + G + B\right)/3\right] \times \pi \qquad \textbf{(9)}$$

By referring to the section 4.3, the critical stress was calculated depending on thermomechanical conditions. Consequently, critical dislocation density (ρ_{cr}) was obtained from;

$$\sigma_{cr} = \sigma_0 + \alpha G b \sqrt{\rho_{cr}} \qquad \textbf{(10)}$$

α, G and b have been defined before. Macroscopically, recrystallization initiated when dislocation density reached a critical amount. But, the microscopic criteria had to be satisfied as well before initiating recrystallization. Therefore, in the next section, the transition rules for recrystallization and dislocation migration in microscopic scale are investigated.

6.2 Stages of Simulation

To get the results from the CA model, there are different stages which should be passed to model recrystallization. The stages of simulation are as follows:

1- An initial microstructure was generated and entered to the CA code which was included the number of grains, the initial average grain size and the orientation of each grain (Figure 12.a).

2- By commencing deformation, hardening was the only deformation mechanism which happened before reaching the critical dislocation density. Therefore, in each time increment a specific amount of dislocation should be added to the microstructure. This amount (Δρ) was obtained from the ρ-t curve (Figure 14). The figure was obtained by knowing that:

$$\sigma = \sigma_0 + \alpha G b \sqrt{\rho} \quad \textbf{(11)}$$

and $\dot{\varepsilon} = \delta\varepsilon / \delta t$ **(12)**

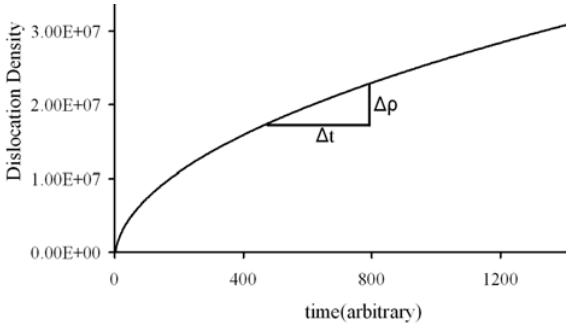

Figure 14. A schematic ρ-t curve. The amount of dislocation which should be dispersed on the domain was calculated from the curve in each time increment.

3- The amount of dislocation which increased due to deformation and hardening (Δρ in Figure 14) was randomly dispersed on the microstructure. As illustrated in Figure 15, the dislocations are distributed randomly while the grain boundaries were distinguished by specific lines and most of the grains have the same amount of dislocations (Figure 15.b). It was supposed that grain boundaries are the energetically barriers for dislocations to migrate from each grain to another one.

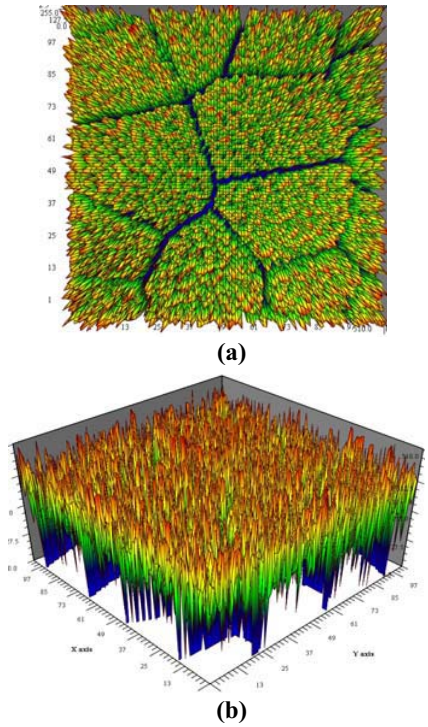

(a)

(b)

Figure 15. Dislocations distribution on the microstructure randomly from top (a), bottom (b) and lateral view (c) respectively.

4- In the same time increment, dislocations migrate along with cells in each grain when the transition rules were satisfied (transition rules of migration will be explained in the following section) to remove any dislocation gradient in each grain. The number of dislocations which could migrate through cells in each grain depended on the dislocation number of sender cell and that of receiver cell.

5- Dislocations accumulated then each cell was checked whether it had equal or higher dislocation density than the critical one (which was calculated from Equation 10).

6- When the dislocation density reached to the critical density, the orientation criterion was checked. By passing both criteria, nucleation initiated in the satisfied cells.

If the number of dislocations in each cell reached the critical value, the cell would change its state from an unrecrystallized cell to the recrystallized one and its dislocation density decreased to the reference level.

6.3 Migration Steps

According to the literature [21], nucleation of new grains take place near grain boundaries. To simulate the recrystallization phenomenon properly, the model should reflect all physical changes by proper transition rules. Transition rules are rules which should be applied on the CA space and they should be satisfied before any transformation in the state of any cell in the CA space [3]. By assuming that dislocations of the cell

A will migrate to the cell B (Figure 16), the transition rules of migration are summarized as following:

a) Cell B is in the neighbourhood of cell A (according to defined neighbourhood radius) (Figure 16) [3]. An important point is that the neighbourhood radius should not be taken very big because the recrystallizing grains will grow quickly and the fully impinged recrystallized microstructure will be obtained while the flow curve showed that the deformation was not completed.

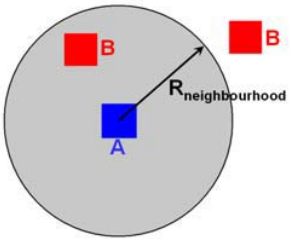

Figure 16. Neighbourhood definition according to the neighbourhood radius.

b) Since, dislocations were able to migrate through the cells whose orientations are the same, therefore, the receiver cell and the sender cell must be located in the same grain and have the same orientation (Figure 12.b).

c) From energy point of view, the total dislocations in cell B should be lower than that in the cell A.

Dislocations migrate from one cell to the adjacent cells which belong to the same grain. However, they cannot cross the grain boundaries. This leads to an increase in the dislocation density near the grain boundaries and triple junctions. It should be noted that triple junctions are more preferable locations for recrystallization than grain boundaries, which has also been replicated in the current model (Figure 17). For instance, three cells considered in three different positions, near triple junction, grain boundary and in the middle of a grain. The neighbourhood radius was assumed constant in the three cases. It is obvious that the cell which is located near triple junction has smaller qualified neighbouring area because one of the criteria for migration was that both cells must be in the same grain (condition b in 6.3). This area would be bigger when a cell is located near a grain boundary and the area would be a complete circle when a cell is in the middle of a grain. Therefore, the cells close to the triple junctions will reach to the critical dislocation density sooner and they will be the first locations in which recrystallization will happen.

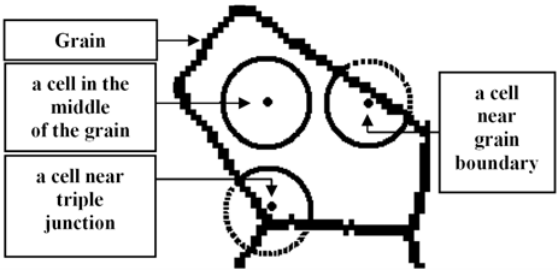

Figure 17. Three cells in different positions, into the grain, near grain boundary and close to the triple junction.

As illustrated in Figure 18, by considering an individual cell in the domain, the number of dislocations increased near grain boundaries and triple junctions when deformation was progressing. So, there was a dislocation gradient between the centre and the margins of each grain (Figure 18). Because of the same reason and considering that triple junctions had higher defect energy than grain boundaries, a large number of dislocations accumulate at these points. Therefore, it would be more preferable for the cells near triple junctions to reach the critical dislocation density than grain boundaries.

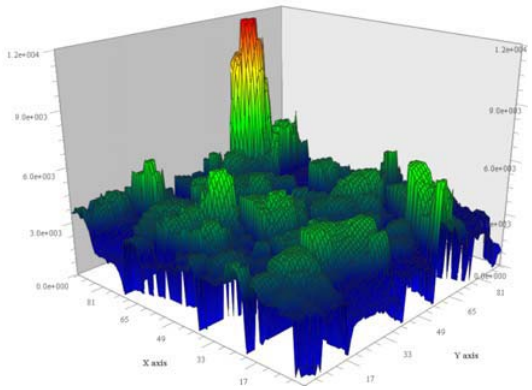

(a)

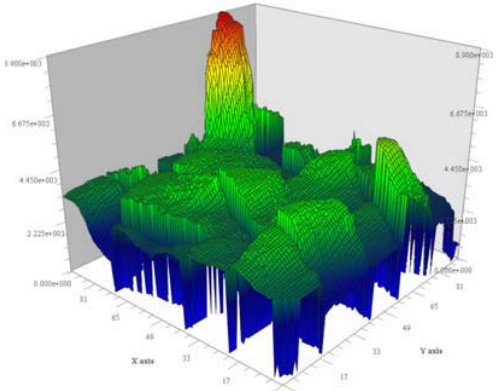

(b)

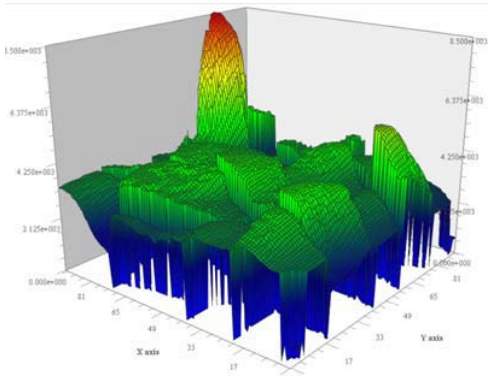

(c)

Figure 18. Dislocation density increased in each grain during deformation and a dislocation gradient was demonstrated in each grain.

By increasing strain, each grain received more dislocations gradually and the number of dislocations in some cells becomes closer to the critical dislocation density (Figure 18.c). Therefore, these cells will be ready to recrystallize and will change their state to the recrystallized state in the next time steps and loose all of their dislocations to the reference level. Also, it was obvious that there was a gradient of dislocations in each individual grain (Figure 18.b,c).

7. NUCLEATION AND GROWTH IN THE CA MODEL

During DRX, various mechanisms are activated and generate new strain-free grains which have high angle grain boundaries during high temperature deformation [22]. Nucleation and grain growth during deformation are assumed as the most general characteristics of DRX once the dislocation density reach to the critical one[23]. Therefore, both nucleation and growth have to be considered as important parts of DRX. Recrystallisation removes the internal energy which was imposed to the material by deformation while the structure was still unstable. But the total internal energy could be reduced by decreasing the total austenite grain boundary area [24]. By giving enough time to the material, the subsequent recrystallized grains will coarsen by grain growth [25]. It is necessary to consider the growth kinetics in the austenite stainless steel which was supported by Sellars [26], Colas [27] and Anan [28]. So, it was essential to model grain growth and its kinetics to verify the microstructure evolution during recrystallization. Siciliano [29] mentioned that growth happened very fast at early stages of growth but it will decrease when time passed. He explained that the rapid grain growth could be due to the high driving force which generated through dislocations existing in dynamically recovered grains.
While deformation is proceeding, the dislocation density exceeds the critical amount. Therefore, nucleation initiates and the satisfied cells will become nuclei and they will nucleate near grain boundaries. At this point, the cells which become new nuclei will set their dislocation level to reference one. But, by continuing deformation and growing the recrystallized cells in the matrix, they can receive more dislocations. Since, the new grain which recrystallized near grain boundary should have the same features of both neighbouring grains on both sides of boundary; the model gives the average orientation of the two neighbouring grains to the new recrystallized grain.
So, growth will continue up to the point in which the dislocation density of recrystallized grain is equal to the matrix dislocation density and the driving force for growth became zero then the growth will cease. While, deformation was proceeding, it could be possible for the recrystallized grains to receive more dislocations and reach to the critical density of dislocation. At this point, the boundary of recrystallized grains can be potential nucleation sites for the second stage of recrystallization. The important point is that the dislocation density which is read from the "ρ-t" curve is a macro-parameter while the dislocation density in each cell is a micro-parameter. To relate them to each other, a mean dislocation density of cells was used to calculate the flow stress of the material. It should be mentioned that the mean dislocation density of all grains was calculated by the following equation in which each cell had a specific fraction of the whole dislocation densities:

$$\rho_{mean} = \sum_i \rho_i \upsilon_i \qquad \textbf{(13)}$$

where ρ_i and v_i were the dislocation density and the volume fraction of the grain i, respectively. By referring to Figure 14.b, the misorientation between two cells in the same grain was equal to zero while it had non-zero value between two cells from two different grains which can be calculated by;

$$\theta=\varphi_1-\varphi_2 \qquad \textbf{(14)}$$

So, the grain boundary energy, γ, can be calculated from the Read–Shockley Equation [30];

$$\gamma = \gamma_m \frac{\theta}{\theta_m}\left(1-\ln\frac{\theta}{\theta_m}\right) \qquad \textbf{(15)}$$

where θ is the misorientation between a grain and its neighbouring grain, γ is the grain boundary energy, γ_m and θ_m are the boundary energy and misorientation respectively when the grain boundary becomes a high angle boundary (in this case, it was supposed higher than 15°). When the growth velocity of a grain calculated, the growth distance in each time increment would be calculated as well. The transformation probability for the site (x,y) which lies in the allowable growth region is determined using cellular automaton method, and the equiaxed growth of grains can be simulated. By calculating the misorientation, it would be possible to calculate the critical dislocation density at the micro-level by the following equation [30]:

$$\rho_c = \left(\frac{20\gamma\dot{\varepsilon}}{3blM\tau^2}\right)^{1/3} \qquad \textbf{(16)}$$

where b is Burger's vector, M is grain boundary mobility, τ is dislocation line energy which is equal to CGb^2 (C is a constant equal to 0.5 and G is shear modulus), and *l* is the dislocation mean-free path which can be taken as the subgrain size. This was calculated by using the following equation:

$$\frac{\sigma l}{Gb} = K_1 \quad \textbf{(17)}$$

where K_1 is a constant close to 10 for metals. γ is also calculated from Equation 15 and grain boundary mobility, M, will be calculated from:

$$M = \frac{\delta D_b b}{KT} \quad \textbf{(18)}$$

where

$$\delta D_b = \delta D_{ob} \exp\left(\frac{-Q_b}{RT}\right) \quad \textbf{(19)}$$

Here δ is the characteristic grain boundary thickness, D_b is the boundary self-diffusion coefficient, Q_b is the boundary diffusion activation energy and K is Boltzmann's constant [11].

By exceeding the critical dislocation density in both micro and macro-levels, the satisfied nuclei started growing and growth will initiate in the coming time steps. By assuming that the recrystallised grains were spherical, the driving force, F, could be measured from the energy changes associated with the growth of the dynamically recrystallized grains. When a nucleus by the radius of "r" grew up by *dr*, the energy change is included two terms. The first term was related to the new surface which is created due to growth and the second term is the volume which is consumed from the neighbouring grains. Therefore, the driving force is a competition between surface and volume energetically which could be expressed as following [30]:

$$dV = dV_{surf.} + dV_{vol.} \quad \textbf{(20)}$$

The change of surface energy was due to the growth of grains and could be defined as:

$$dV_{surf} = d\left(4\pi r^2 \gamma\right) = 8\pi r \gamma dr \quad \textbf{(21)}$$

The change of volume energy is due to the consuming the previous grains and can be expressed as:

$$dV_{vol} = \tau(\rho_d - \rho_m) \times \left(\frac{4}{3}\pi(r+dr)^3 - \frac{4}{3}\pi r^3\right) = 4\pi r^2 \tau(\rho_d - \rho_m) dr \quad \textbf{(22)}$$

The driving force was defined as following:

$$F = -\frac{dV}{dr} = 4\pi r^2 \tau(\rho_m - \rho_d) - 8\pi r \gamma \quad \textbf{(23)}$$

where ρ_m and ρ_d were dislocation densities of the matrix around the growing grain depending on the neighbourhood definition and that of the dynamically recrystallised grain. According to the Equation 23 growth will continue up to the point that F becomes zero after which growth stopped. The constants which were used in the CA model are summarized in the table 3.

Table 3 The values of input data or constants used in the CA model.

Parameter	b(m)	Q_b (KJ/mol)	δD_{ob} (m^3/s)
Value	$2.5*10^{-10}$	174	$1.1*10^{-13}$
Parameter	γ_m (mJ/m^2)	K($J/^ok$)	
Value	$8.35*10^{-7}$	1.38×10^{-23}	

8. MODEL VERIFICATION

By applying the criteria and transition rules which were attempted to duplicate the physical concepts of recrystallization to the CA model, the model produced a microstructure which is shown in Figure 12. The final results should be verified from two points of view, mechanical behaviour of material (flow curve) and metallurgical view (final microstructure, average final grain size and texture).

According to literature [31], the initial grain size only affected the general shape of flow curves very little. The influence of initial grain size at different strain rates (when temperature is constant) was similar to the effect of temperature (when strain rate is constant). In the case of coarse-grained material, the delay in the initiation of DRX gives more time to recovery to take place. Therefore, two different initial microstructures with different initial grain sizes were investigated. By considering 20 μm and 35 μm as the initial grain sizes and the same deformation schedule (constant strain rate and temperature), the model should result the same final grain size. Two stress-strain curves which were related to the two different initial grain sizes have been considered (Figure 19).

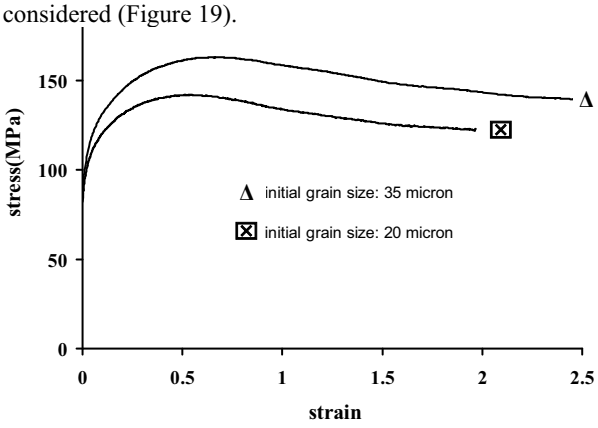

Figure 19. Stress-strain curve for two different initial average grain sizes.

After running the CA model, the stress-strain curves have been derived from the ρ-t curve and final microstructures have been obtained. Figure 20 shows the "dislocation density-time" curve obtained from the simulation. It demonstrated that up to the peak stress,

simulation and experimental results have an accurate agreement. By continuing the deformation, the deviation from the experimental results was increased. One of the reasons could be the difficulties to reflect the grain growth phenomenon on the CA model properly.

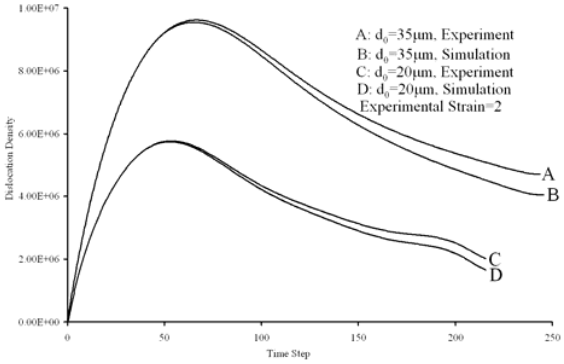

Figure 20. comparison of ρ-t curves in two different initial average grain sizes from experiments and simulation.

As it is obvious, after peak stress, there is some under-estimation which is related to the growth of new recrystallized grains but the final microstructures obtained from the simulation gave better results in comparison with mechanical behaviour. The experimental results from torsion test shows that the final microstructure with the same thermomechanical condition has an average grain size of 10.5 μm (Figure 21).

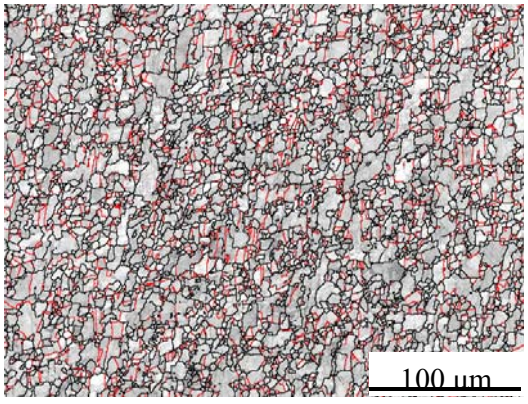

Figure 21. Microstructure from hot torsion test in T=900 ^{0}C, ε̇=0.01 S^{-1}

By comparing the results from the simulations, it is revealed that when the initial grain size is 35 μm, the final grain size is 10.7 μm while it is 10.3 when a microstructure with the 20 μm grain size was used (Figure 22).

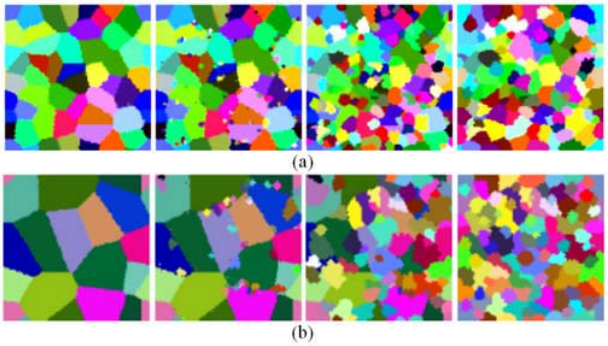

Figure 22. comparison two final microstructure when the initial grain size in different. d_0=20 μm (a), d_0=35 μm (b).

As dynamic recrystallisation progressed during deformation, work hardening occurred within the recrystallized grains. Therefore, the driving force for growth reduced and limited the maximum size of the recrystallized new grains. When Z value is high enough, the final grain size will be determined by the work hardening which controlled the growth rate. If the work hardening rate is low enough, there will be enough driving force for growth and the grains grow continuously before the point in which dislocation density in the grain reduced the growth rate. Therefore, the grain boundaries will be limited when they met each other when impinged recrystallized grains face to each other. Thus, the final grain size will be controlled by the number of other recrystallized grains which were competing to consume the initial microstructure [32].

9. CONCOLUSION

The hot torsion test of a 304 austenitic stainless steel was investigated to predict dynamic recrystallization curve through Estrin-Mecking theory and through numerical approach. Considering no effect of initial grain size on the final microstructure, two different initial grain sizes were used to validate the CA model. The most important results experienced in this study can be summarized as following:

i. The Estirn-Mecking theory can properly represent dynamic recovery in the present material.
ii. The numerical approach shows a good agreement with the EM theory. So, by defining thermomechanical conditions, the dynamic recovery curve can be obtained from the numerical approach.
iii. Peak, critical and steady state stresses (derived from the analysis) showed power law functions with Zener-Hollomon parameter.
iv. The microstructure derived from the CA model has the same final average grain size as calculated from experiments.
v. The CA model illustrated that final grain size just depends on deformation conditions and is independent of the initial grain size.

Acknowledgements

This research was supported by grants through ARC (N.Yazdipour) including an ARC federation fellowship (P.D.Hodgson).

References

1. H. McQueena, C.A. Imbert, *Journal of Alloys and Compounds*, 2004, vol.378, pp. 35-43.
2. H.W. Hesselbarth, I.R. Gobel, *Acta metal. & Mater.*, 1991, vol. 39, pp. 2135-2143.
3. G.F.J. Koenraad, *Modelling and simulation in Mat. Scie. and Eng.*, 2003, vol. 11, pp. 157-171.
4. F.J. Humphreys, M. Hatherly, "*Recrystallization and Related Annealing Phenomena*", 2nd,1996, pp. 188-216
5. E.I. Poliak, J.J. Jonas, ISIJ, 2003, vol. 43, pp. 684-691.
6. H. Mecking, U.F. Kocks, *Acta Metal*., 1981, vol. 29, pp. 1865-1875.
7. Y. Estrin, H. Mecking, *Acta Metall.*, 1984, VOL. 32, pp. 57-70.
8. Y. Estrin, *Unified Constitutive laws of Plastic Deformation*, 2nd ed., A.S. Krausz, ed., K. Krausz, Ontario, 1996, pp. 68-105.
9. A. Belyakov, T. Sakai, H. Miura, R. Kaibyshev, K. Tsuzaki, *Acta Mat.*, 2002, vol. 50, pp. 1547-1557.
10. R. DING, Z.X. GUO, *Acta Mater.*, 2001, vol. 49, pp. 3163-3175.
11. R. Ding, Z.X. Guo, *Comp. Mat. Sci.*, 2002, vol. 23, pp. 209-218.
12. P.D. Hodgson, *PhD Thesis*,1993, University of Queensland
13. S.H. Zahiri, C.H.J. Davies, P.D. Hodgson, *Scripta Mater.*, 2005, vol. 52, pp. 299-304.
14. H.J. McQueen, N.D. Ryan, *Materials Science and Engineering A*, 2002, vol. 322, pp. 43-63.
15. N.D. Ryan, H.J. McQueen, *Canadian Metallurgical Quarterly*, 1990, vol. 29, pp. 147-162.
16. E.I. Poliak, J.J. Jonas, *Acta Mater.*, 1996, vol. 44, pp. 127-136.
17. Davenport, Silks, Sparks, Sellars, *Mat. Sci. and Tech.*, 2000, vol. 16, pp. 539-546.
18. C. Roucoules, P.D.Hodgson, S. Yue, J.J. Jonas, *Met. and Mat. Transaction A*, 1994, vol. 25A, pp. 389-400.
19. D. Raabe, *Annu. Rev. Mater. Res*, 2002, vol. 32, pp. 53-76.
20. G.F.J. Koenraad, "*Continuum scale simulation of Engineering materials; fundamentals, microstructures ,process applications"*, ed., D. Raabe, F. Roters, F. Barlat, L.Q. Chen, 2004, chap.12.
21. D. Raabe, M. Sachtleber, Z. Zhao, F. Roters, S. Zaefferer, *Acta Mat.*, 2001, vol. 49, pp. 3433-3441.
22. D.Q. Bai, S. Yue, J.J. Jonas, *1st International Conference on Modelling of Metal Rolling Processes*, 1993, pp. 180-184.
23. Andrade, M.G. Akben, J.J. Jonas, *Met. Trans. A*, 1983, vol. 14A, pp. 1967.
24. Kwon, Deardo, *Acta Metal. & Mater.*, 1991, vol. 39, pp. 529-538.
25. P.D.Hodgson, R.K. Gibbs, *ISIJ*, 1992, vol. 32, pp. 1329.
26. C.M. Sellars, *7th Int. Symp. on Metallurgy and Materials Science*, 1986, pp. 167-187.
27. Colas, *Mat. Sci. and Tech.*, 1998, vol. 14, pp. 388-393.
28. Anan, Nakajama, Miyahara, Nanba, Umemeto, Hiramatsu, Moriya, Watanabe, *ISIJ*, 1992, vol. 32, pp. 262-266.
29. A. Kirihata, F. Siciliano, T.M. Maccagno, J.J. Jonas, *ISIJ*, 1998, vol. 38, pp. 187-195.
30. R. Ding, Z.X. Guo, *Comp. Mat. Sci.*, 2002, vol. 23, pp. 209-218.
31. T. Sakai, M.G. Akben, J.J.Jonas, *Acta Metal.*, 1983, vol. 31, pp. 631-642.
32. T. Sakai, J.J. Jonas, *Acta metal.*, 1984, vol. 32, pp. 189-209.